NASA TECHNICAL MEMORANDUM

NASA TM X-73646

NASA TM X-73646

ULTRASONIC EVALUATION OF THE STRENGTH OF UNIDIRECTIONAL GRAPHITE-POLYIMIDE COMPOSITES

by A. Vary and K. J. Bowles
Lewis Research Center
Cleveland, Ohio 44135

TECHNICAL PAPER presented at the
Eleventh Symposium on Nondestructive Evaluation
cosponsored by the American Society for Nondestructive Testing and the Southwest Research Institute
San Antonio, Texas, April 20-22, 1977

ULTRASONIC EVALUATION OF THE STRENGTH OF UNIDIRECTIONAL GRAPHITE-POLYIMIDE COMPOSITES

A. Vary and K. J. Bowles
Lewis Research Center
Cleveland, Ohio 44135

Abstract

This paper describes an acoustic-ultrasonic method that was successful in ranking unidirectional graphite-polyimide composite specimens according to variations in interlaminar shear strength. Using this method, a quantity termed the "stress wave factor" was determined. It was found that this factor increases directly with interlaminar shear strength. The key variables in this investigation were composite density, fiber weight fraction, and void content. The stress wave factor and other ultrasonic factors that were studied were found to provide a powerful means for nondestructive evaluation of mechanical strength properties.

E-9153

A. SUMMARY

Specimens of a unidirectional graphite-polyimide (AS/PMR-15) fiber-reinforced composite were fabricated by using various cure pressures. A range of void-contents and fiber-to-resin ratios were obtained for a series of these laminates. There were corresponding variations in mechanical strength properties. The specimens were evaluated nondestructively and then subjected to mechanical destructive testing.

The most significant finding was a strong correlation of the ultrasonically-measured quantity, termed the "stress wave factor", ϵ_{sw}, with the interlaminar shear strength, τ_{il}. The quantity ϵ_{sw} was determined by a novel acoustic-ultrasonic nondestructive method. The shear strength was obtained by means of short-beam shear tests. The quantity ϵ_{sw} is a measure of the relative efficiency with which stress wave energy will propagate in a given specimen. This quantity is apparently determined by microstructural features such as void distribution and shape and fiber-to-resin ratio variations.

The ultrasonic modulus ρv^2, based on density and velocity measurements, respectively, was also compared with interlaminar shear strength. Again, strong correlations were found. In general, the results of this study indicate that the acoustic-ultrasonic methods described herein can form a powerful tool for nondestructive determination of factors that influence the mechanical strength of composite structures. A method for rating or estimating interlaminar shear strength using only ultrasonic measurements is described.

B. INTRODUCTION

There is a need for nondestructive evaluation (NDE) techniques that go further than simply finding overt flaws in composite structures.[1] Even when such flaws are absent there can be serious strength and endurance deficiencies. Some of these arise during fabrication while others arise from use and exposure. Therefore, this paper describes work that concentrated on investigation of NDE techniques that can (indirectly) measure variations in strength-related properties. Pertinent factors that should be included in studies of this type include micro-voids and fiber-to-resin variations distributed throughout a composite structure.

Currently available nondestructive evaluation methods for composite structures usually fail to adequately predict mechanical property variations. Typically, they yield only qualitative data relative to strength.

A need was perceived for a new acoustic ultrasonic method for sensing and measuring variations in composite strength due to the previously-mentioned factors. It was thought that this new method should measure the relative efficiency with which stress waves will propagate in a given composite structure. The working hypothesis was that the presence of

STAR category 38

micro-voids, for example, reduce both the composite's strength and also the stress wave propagation efficiency. The prime purpose of the work reported herein was to test this hypothesis for a series of graphite-polyimide laminate specimens.

It should be noted that ultrasonic methods have been used previously to determine elastic modulus, void content, and like factors.[2,3,4,5] However no prior method is known to be able to yield the strength correlations discovered in this study. Moreover, we were particularly interested in a tool for ranking the relative strength of composite structures with a simple contact probe configuration requiring only one side access. This was to assure easier adaptability to more complex parts while being able to measure significant strength-related factors.

C. SYMBOLS

NOTE: Dimensions used in text are given following the symbol definition.

b	specimen width, cm
ε_{sw}	stress wave factor
f_f	weight fraction of fiber
f_r	weight fraction of resin
k_f	fiber volume fraction, $= f_f\rho_c/\rho_f$
k_r	resin volume fraction, $= f_r\rho_c/\rho_r$
k_v	void volume fraction, eq. (2)
L	breaking load, MN
P	cure (die) pressure, MPa
t	specimen thickness, cm
v_ℓ	through thickness velocity, cm/μs
v_s	surface parallel velocity, cm/μs
α_ℓ	attenuation coefficient, Np/cm
ρ_c	density of composite, g/cm^3
ρ_f	density of fiber, = 1.799 g/cm^3
ρ_r	density of resin, = 1.313 g/cm^3
τ_{il}	interlaminar shear strength, MPa
$\langle\tau_{il}\rangle$	shear strength estimator, MPa

D. EXPERIMENTAL PROCEDURE AND RESULTS

1. General Approach

An appropriate composite fiber-resin system (AS graphite-PMR polyimide) was selected, and unidirectional flat panel laminates were fabricated. The selection was based on technical interest and potential use in aircraft engine components.

The panel laminates were made with virtually identical physical dimensions. The (micro-) void content and fiber/resin ratio were intentionally varied from panel to panel. After fabrication, each specimen panel was examined with appropriate nondestructive methods and the results were documented. Following this, small sections were taken from the panels and these were subjected to various destructive tests. Properties that were destructively measured included interlaminar shear strength, density, void fraction, and fiber weight fraction. These results were compared with the nondestructive test indications, and significant correlations were analyzed.

2. Specimens

a. Panel Fabrication

Eleven 12-ply unidirectional panel laminates were made with a range of cure pressures. Using only the cure pressure as a fabrication variable, it was possible to produce a significant range of void contents and fiber/resin ratios. Fabrication details are given in Appendix A. The cure pressure used for each panel and material properties based on specimens taken from the panels are indicated in table I.

b. Specimen Description

Figure 1 depicts overall dimensions of the laminate panels and the fiber orientation. A 1.59 cm (0.625 in) wide strip (the "E-strip" in fig. 1) was taken from each of the 11 panels made. The E-strip yielded the short beam shear and other specimens discussed in this report. The remainder of each panel was reserved for other experimental uses (not reported herein). The scheme for excision of short beam shear specimens is diagrammed in fig. 1(b). Other portions of the E-strip served as sources for density, metallographic, and other measurements.

As indicated in fig. 1(b) the E-strip was divided into 10 sections with the letter designations K through T. After nondestructive examination, these yielded the short beam shear specimens. These specimens were cut out so that the long edge of the specimen was parallel to the fiber direction. All cutting was done with a water-cooled diamond wheel. Each of the sections, marked K through T, produced two samples. One of these, measuring about 0.508 cm (0.200 in) in width and 1.58 cm (0.625 in) in length, was used in the short beam shear tests. The second sample, measuring about 0.450 cm (0.180 in) in width was saved for later evaluation. It represented as-cured material and was reserved to clarify any discrepancies or unusual test results obtained with the first sample. Since the two samples were cut from each of the lettered sections of the E-strip, there were altogether twenty samples available. The E-strip from panel P21 was an exception to this. Because of breakage, P21E yielded only five pairs of samples.

3. Nondestructive Evaluations

a. Ultrasonic Scanning

Two types of ultrasonic mappings were made for each panel: a greytone scan and an amplitude scan. Typical results are shown in fig. 2. These scan images are both based on transmission of ultrasonic signals through the panels. The ultrasonic scans clearly show variations in ultrasonic attenuation due to various factors such as voids, delaminations, resin-rich regions, etc. Amplitude scans for panels made with three different cure (die) pressures are shown in fig. 3. Greater attenuation corresponds to a lower signal levels in the amplitude scans and whiter areas in the greytone scans, fig. 2.

The scanning was done with the panels immersed in distilled water. They were positioned between two opposing ultrasonic transducers: one sending, the other receiving. Both had a nominal center frequency of 2.25 MHz. The panels were all scanned using identical instrument settings, e.g., gain, damping, filter, etc. Thus, all the scans were made with reference to exactly the same baseline condition or zero reference level, indicated in fig. 2(d). (The zero reference level is an instrument setting at the noise threshold.)

b. Velocity and Attenuation

Spot or localized sampling measurements of attenuation and velocity were also made using contact ultrasonics. Through-the-thickness velocity and attenuation measurements were made on the E-strips according to the schemes shown in fig. 4. Details for making these measurements are given in Appendix B.

The results of the spot attenuation measurements agreed with the scan image results. Obviously, the scan images complement the spot measurements by mapping the continuity of attenuation variations. Mean measured values of velocity and attenuation for the E-strips are presented in table II.

In addition to velocity measured through-the-thickness, v_ℓ, velocity of sound was measured parallel to the surface, v_s. In either case, the velocity of propagation was perpendicular to the fiber direction. The surface-parallel velocity, v_s, was measured using a method similar to that reported in[4,5]. In the present case, the apparatus was different in important respects. This apparatus is illustrated in fig. 5 and discussed in Appendix C.

c. Stress Wave Simulation Method

The stress wave simulation method produces a measurement of the "stress wave factor", ε_{sw}. This factor was determined for a series of local areas on each E-strip. The method is illustrated in fig. 6 and explained in Appendix D. The method depends on mimicing stress wave events in the material[6,7] and using the resultant "simulated" stress waves to evaluate properties that correlate with wave propagation phenomena.

It is possible to measure this stress wave factor in three directions relative to the (unidirectional) fibers: (1) longitudinally, parallel to the fibers with both probes on one side as in fig. 6(a); (2) transversely, perpendicular to the fibers (again with probes on one side); and (3) transversely, through the laminate thickness with probes on opposite sides. All the ε_{sw} values quoted herein were measured transversely to the fibers, as in case (2).

Stress wave factor measurements were made on each E-strip with one measurement for each of the ten lettered sections K through T (K through O for P21E), see fig. 1. Three additional random measurements were made for each E-strip. The mean value of the stress wave factor for each E-strip is given in table II.

4. Material Property Measurements

a. Interlaminar Shear Strength

All interlaminar shear tests were made at room temperature using a three-point loading fixture with a constant span/depth ratio of 5. The rate of loading was 0.02 cm/s (0.5 in/min). Ten specimens were cut from each test panel (E-strip). The short-beam shear specimen thickness varied from 0.23 cm to 0.25 cm (0.09 in to 0.10 in). These specimens were all 0.508 cm (0.200 in) wide. The formula used to calculate the interlaminar shear strength from the test data is,

$$\tau_{il} = 0.75\ L/bt \qquad (1)$$

where, τ_{il} is interlaminar shear strength, L is breaking load, b is specimen width, and t is specimen thickness.

The method for conducting short beam shear tests is set forth in[8]. The interlaminar shear values reported herein are arithmetic means of the ten values measured for each E-strip. The sole exceptions was P21E which yielded only five short-beam shear specimens. These mean values are tabulated in table I.

b. Composite Density

Density measurements were made gravimetrically on the short-beam shear specimens by computing from weight and dimensions and also by immersion in distilled water. After the short beam shear tests were completed, density measurements were repeated using the 0.450 cm (0.180 in) wide companion sample from each of the lettered sections from the E-strips (described previously). These densities were measured using methyl alcohol as the immersion

liquid. The average variation in measured density among the three different methods was about ±1 percent.

c. Fiber Fraction

After loading to fracture, fiber content was determined for three short-beam shear specimens from each E-strip. This was done to determine fiber and resin weight fractions. For all strips except P21E, these samples were taken from sections L, P, and S. In the case of P21E the fiber weight fraction was determined from sections L and O. The fiber content was determined by resin digestion in concentrated sulfuric acid. The acid digestion method is discussed in[9]. Results of the various density measurements and fiber and resin weight fraction determinations appear in table I.

d. Void Content

The void content of each of the specimens tested was calculated from the density measurements described previously. The calculation was made by taking,

$$k_v = 1 - \rho_c(f_f/\rho_f + f_r/\rho_r) \quad (2)$$

where, k_v is void volume fraction, ρ_c is density of the composite, ρ_f is density of the fiber (= 1.799 g/cc), ρ_r is density of the resin (= 1.313 g/cc), f_f is weight fraction of fiber, and f_r is weight fraction of resin. The value for the fiber density was obtained from the manufacturer's data sheet. The value for the resin density was measured by water immersion of a resin sample. The reliability of the void content determination used is discussed in[10,11]. The method is not accurate for void contents of less than roughly 1 percent. Therefore, all values less than 1 percent calculated from eq. (2) were set equal to zero. This value was confirmed by metallography that showed there were actually no voids in the corresponding samples. The mean void content for each E-strip is given in table I.

e. Metallography

Three samples of the as-cured and untested material were taken from the L, P, and S areas of each E-strip. The exception was P21E where samples were taken from the L and O areas. The samples were mounted, polished, and photographed at various magnifications, X30 to X160, to confirm the void size, distribution, and shape. Typical photomicrographs appear in fig. 7. In addition, one or two of the short-beam shear specimens from each E-strip were examined metallographically to determine the failure mode. In those cases where unusually high or low shear strength value was measured relative to the mean, two samples were examined. One sample represented the mean shear strength, and the other was the one that produced the unusual deviation.

E. ANALYSIS OF RESULTS

5. Overview

a. Organization

The experimental results are analyzed in the following order: First, we examine the interrelations among key physical factors that affected the interlaminar shear strength, τ_{il}, of the composites. These physical factors are composite density, ρ_c, fiber weight fraction, f_f, and void volume fraction, k_v. Second, we examine empirical correlations between τ_{il} and ultrasonic factors such as the ultrasonic moduli $\rho_c v_\ell^2$ and $\rho_c v_s^2$, attenuation coefficient α_ℓ, and the stress wave factor ϵ_{sw}. Third, we describe an empirical method for estimating interlaminar shear strength from measurements of ϵ_{sw} and v_s.

b. Preliminary Observations

Examination of the panels with ultrasonic scanning revealed significant variations in transmission: lower cure pressures resulted in panels that were more attenuating to ultrasound, see fig. 3. Furthermore, lower cure pressures produced panels that exhibited considerably more attentuation "peaks" and "valleys". For the highest cure pressures, >3.5 MPa (>500 psi), the scans showed a uniform level of attenuation, see fig. 3(a). For intermediate cure pressures, about 1.4 MPa (200 psi), variations in attenuation gave evidence of variable density essentially parallel to the fibers, see fig. 3(b). This resulted in various fiber-rich and void-rich areas. In the curing process, voids are not generated with PMR resin. Resin flow sweeps out entrapped gas initially present in the imidized preform. For pressures below approximately 3 MPa, the density depends on resin distribution. Above approximately 3 MPa, the density depends on fiber packing. For the lowest cure pressures, 0.7 MPa (100 psi), resin flow was less and hence fiber-rich and void-rich areas were more pronounced, see fig. 3(c). Higher cure pressure resulted in more resin flow.

Fiber-richness or high fiber volume fraction was associated with best transmission while high resin and/or void fractions resulted in more attenuation of ultrasound. The patterns of attenuation seen in the scan images give a qualitative indication of the acceptability (integrity) of the composite structure. A through-transmission ultrasonic method for qualitatively ranking composite according to void fraction and associated strength variations is discussed in[2,3].

c. Note Concerning Graphs

In all the graphs, figs. 8 through 15, the data points are labeled to indicate the panel E-strip from which the data came. Thus, each plot will contain 11 data points corresponding

to the E-strips P20E through P30E. These labels will facilitate cross referencing with values given in tables I and II. In addition, in each graph the data are represented by 3 different symbols. Each symbol corresponds to a particular range of fiber weight fraction values: 0.60 to 0.62, 0.62 to 0.64, and 0.64 to 0.66. This was done to facilitate analysis of the effect of fiber content. Note that each data point on the graphs generally represents the arithmetic mean of ten separate measurements.

6. Material Property Correlations

a. Shear Strength Factors

It is natural to expect that higher fiber content (high values of f_f) should be accompanied by higher composite strength (up to a specific value of void content). After this, the strength would decrease. This expectation is supported by fig. 8 where interlaminar shear strength, τ_{il} is plotted against void content, k_v. (In this study the optimum fiber content for maximum τ_{il} was not obtained.) In their combined effect on τ_{il}, it is inferable from fig. 8 that f_f has a greater relative influence than k_v, at least for k_v less than about 8 percent (the curves in fig. 8 intersect at k_v of about 8%). Thus, one would attribute a greater importance to the mechanical strength or stiffness of the fibers at least for low void fractions. This agrees with the contention of ref. 12 (p. 11) relative to the influence of fiber strength on interlaminar shear tests.

b. Shear Strength and Density

Various theoretical attempts have been made to predict the combined effect of fiber and void fractions on strength[13,14]. It will be seen that composite density is a remarkably good predictor of interlaminar shear strength. This is evident in fig. 9. It is noteworthy that f_f and k_v are intrinsically contained in ρ_c,

$$\rho_c = (1 - k_v)/(f_f/\rho_f + f_r/\rho_r) \qquad (3)$$

where eq. (3) follows from eq. (2) and $f_r = (1 - f_f)$. The data in fig. 9 can be taken as falling on a single line.

7. Ultrasonic-Acoustic Correlations

a. Attenuation Coefficient

Through-the-thickness ultrasonic attenuation was determined by two methods: scanning and spot measurements. Qualitatively, the results of the two methods agreed reasonably well. The latter method gave numerical attenuation coefficient, α_ℓ, values. These are compared with interlaminar shear strength values in fig. 10. Although there is considerable scatter, it is clear that higher attenuation coefficients were associated with lower strength, τ_{il}. The magnitude and amount of scatter of α_ℓ relative to τ_{il} resemble the findings reported in[2] for a similar composite. For various reasons the correlation between α_ℓ and τ_{il} is not very strong for the materials tested in this study (see Micrographic Observations).

b. Ultrasonic Moduli

The ultrasonic modulus ρv^2 corresponds to the tensile modulus E through the approximate relation $v^2 \sim E/\rho$. (A factor involving Poisson's ratio is omitted.) We can, therefore, form the products $\rho_c v_\ell^2$ and $\rho_c v_s^2$ with the expectation that they might correlate with strength. Figures 11 and 12 show the results of plotting τ_{il} as a function of $\rho_c v_\ell^2$ and $\rho_c v_s^2$, respectively. Both the through-transmission and surface-parallel velocities, v_ℓ and v_s, were measured with waves traveling in a direction perpendicular to the fibers.

The strong correlation apparent in figs. 11 and 12 are interesting in two respects: First, we find that τ_{il} varies directly with $\rho_c v_\ell^2$ and inversely with $\rho_c v_s^2$. Second, we note that in each figure the data divide into two groups. Data points 20, 21, 22, 25, and 30 are in Group A while 23, 24, 26, 27, 28, and 29 are in Group B. This separation into two populations is indisputable in fig. 11 and is statistically supportable in fig. 12.

The grouping of τ_{il} versus $\rho_c v_\ell^2$ and $\rho_c v_s^2$ data is apparently controlled by void content. Points 20, 21, 25, and 30 of Group A are essentially void-free with $k_v < 1\%$. Points 24, 26, 27, and 29 of Group B have $k_v \geq 4\%$. For points 22 of Group A and points 23 and 28 of Group B we have $1\% < k_v < 4\%$. These three specimens apparently belong to a transitional population. Our interpretation is that τ_{il} of Group A is controlled predominantly by the fibers (i.e., fiber stiffness or modulus) while in Group B the voids are slightly more significant in controlling τ_{il}.

If $\rho_c v_\ell^2$ and $\rho_c v_s^2$ are interpreted as being proportional to the mechanical modulus[1,4,5], then these moduli are clearly functions of f_f and k_v by eq. (3). The quantity $\rho_c v_\ell^2$ is probably an inter-laminar tensile modulus while $\rho_c v_s^2$ is probably an inter-laminar shear modulus. This assumption might account for the direct and inverse relations with respect to τ_{il} in figs. 11 and 12, respectively.

c. Stress Wave Factor and Strength

The wave injected in the process of measuring the stress wave factor, ε_{sw}, resembles a stress wave that would arise during microfracture (see (6,7) and Appendix D). Lower values of the quantity ε_{sw} probably correspond to greater dissipation of energy as a stress wave propagates through a material. Our working hypothesis was that the variations in void and fiber fractions affect both composite strength and also actual stress wave propagation during

microfracture. Then, measuring the quantity ε_{sw} should yield data that correlates with properties that influence crack propagation and hence strength.

The above hypothesis is supported by the results shown in fig. 13. Therein, the interlaminar shear strength τ_{il} is plotted as a function of the stress wave factor ε_{sw}. The data can be divided into two populations indicated by the curves marked U and L in fig. 13. Regression analysis for each curve gives a high coefficient of correlation, i.e., for each it is 0.98. If all other data points are assumed to belong to the same population, then point 28 is a "maverick". It is significant that this point represents ten specimens that had the lowest mean fiber fraction f_f. Note that 28 belongs to a previously identified "transitional" set of specimens (22, 23, 28).

Figure 14 exhibits the correlation between composite density, ρ_c, and the stress wave factor, ε_{sw}. As was mentioned before, ρ_c is a function of k_v and f_f, eq. (3). It is evident from fig. 14 that the ρ_c versus ε_{sw} data are isometric with respect to τ_{il}. The plot of fig. 14 consists of a family of lines, each one corresponding to a particular interlaminar shear strength. The "transitional" points 22, 23, and 28 are now seen in a different context: It is obvious in fig. 14 that there are no "maverick" points when using this indirect method of plotting τ_{il} against ε_{sw}.

d. Micrographic Observations

Microscopic examination of the short beam shear specimens showed that they also divided into two groups. One group (related to curve U in fig. 13) exhibited evidence of flexure and fiber tearing on the tensile side, see fig. 7(c). The other group (related to curve L in fig. 13) gave no evidence of flexure while clearly showing interlaminar failure effects, see fig. 7(d). (See DISCUSSION for limitations on these conclusions.)

Examination of figs. 7(a) and 7(b) reveals that the void content consisted of two essentially different kinds of voids: cracklike and pinhole. Hence, the value of k_v is composed of two components. This may explain why the ultrasonic attenuation coefficient did not correlate strongly with interlaminar shear strength in fig. 11. This lack of strong correlation may be because α_ℓ is more sensitive to void size and shape than τ_{il}.

8. Estimating Interlaminar Shear Strength

a. Key Ultrasonic Factors

It is possible to determine τ_{il} using only ultrasonic data measured by one side access to the specimen. Plotting v_s^2 versus ε_{sw} results in a family of lines each of which is associated with a particular value of τ_{il}, see fig. 15(a).

Note that in fig. 15(a) the lines converge to a common point and that their angular spacing is systematic. It is easy to interpolate to infer positions of intermediate lines in the family. Given the full family of lines, pairs of values v_s and ε_{sw} will uniquely determine τ_{il}. It will be noticed that fig. 15(a) resembles an inverted version of fig. 14(c). This is the consequence of the fact that v_s and ρ_c are empirically related.

b. Empirical Equations

Inspection of fig. 15(a) suggests that the relation among τ_{il}, ε_{sw}, and v_s can be expressed by,

$$(4) \qquad \tau' = 114 \cos \text{arc tan} \times [10^3(v_s^2 - 0.0144)/(3.10 - \varepsilon_{sw})]$$

where, τ' is an estimator of τ_{il}. The factor 10^3 in the brackets is an arbitrary proportionality constant needed to adjust for the difference in coordinate scales between v_s^2 and ε_{sw} in fig. 15(a). This proportionality constant is arbitrary because ε_{sw} is a pure number having no intrinsic magnitude. Figure 15(b) is a plot of τ_{il} against τ'. This relation between τ_{il} and its estimator, τ', can be linearized by finding a regression curve to fit the points of fig. 15(b). One such curve is given by,

$$(5) \qquad \langle \tau_{il} \rangle = 35.30 + 16.71 \ln \tau'$$

where, $\langle \tau_{il} \rangle$ is the new estimator for τ_{il}. Figure 15(c) shows the resulting relation between τ_{il} and $\langle \tau_{il} \rangle$.

Since the choice of the scaling factor in eq. (5) is arbitrary, it can be adjusted to accommodate the data in order to improve the linearization of the τ_{il} against $\langle \tau_{il} \rangle$ relation. Also, we can begin with a plot of v_s against ε_{sw} instead of v_s^2 against ε_{sw}. The new plot (v_s vs. ε_{sw}) will be similar to fig. 15(a). Using this approach, one can modify the expression for the estimator $\langle \tau_{il} \rangle$ to get,

$$(6) \qquad \langle \tau'_{il} \rangle = 47.21 + 14.46 \ln \times \{114 \cos \text{arc tan}[400(v_s - 0.12)/(3.1 - \varepsilon_{sw})]\}$$

The result of comparing τ_{il} to $\langle \tau'_{il} \rangle$ is shown in fig. 15(d). In that figure the scatter and hence error of estimate is considerably less than in the previous figure.

F. DISCUSSION

It is apparently possible to estimate the relative mechanical strength of a composite material by using only ultrasonic-acoustic measurements. Moreover, in this study the necessary measurements were obtained with methods requiring access to only one surface of the specimens investigated. In fig. 13, the available ultrasonic data appear to define an "upper bound"

and "lower bound" curve, U and L, respectively. Thus the stress wave factor, ε_{sw}, alone (as in fig. 13) can always be used to give a conservative estimate of τ_{il} by using the lower bound curve. Note that ε_{sw} is both a sufficient estimator of τ_{il} and also a considerably easier one to determine than the other ultrasonic quantities, e.g., v_ℓ and especially v_s.

If v_s is measured in addition to ε_{sw}, then τ_{il} can be uniquely determined as in fig. 15(a). By compiling sufficient data on a particular composite material, it is possible to generate empirical equations giving τ_{il} as a function of ε_{sw} and v_s, as in eqs. (4) through (6). It should be recognized that the functional forms of eqs. (4), (5), and (6) can not be assumed to have physical significance. They are merely results of graphical and statistical manipulations to express empirical correlations.

All ultrasonic measurements were made within a narrow frequency domain, i.e., between 0.1 MHz and 2.5 MHz, approximately. Different results should be expected in case of substantially different frequency domains. The previously mentioned domain (0.1-2.5 MHz) was determined to be suitable for the composite material studied. The main criterion was that the wave length be of the order of the specimen thickness. This criterion was based on practical considerations. Frequencies much higher than about 2.5 MHz would not yield good ultrasonic measurements for the full range of specimen conditions. The attenuation would be too high for specimens with the higher void contents. Frequencies much lower than 0.1 MHz would not produce wave interactions appropriate to the specimen microstructure.

The results reported herein are associated with the particular materials, fiber orientation, and fabrication process used. It is probable that the relations discovered apply generally. However, all the empirical equations relating τ_{il} to various ultrasonic terms, e.g., $\rho_c v_\ell^2$, $\rho_c v_s^2$, and ε_{sw}, should be taken only as illustrative examples. In particular, the stress wave factor, ε_{sw}, will be strongly influenced by geometric features peculiar to a given composite structure and by different orientations of the probes. Note also that both quantities v_s and ε_{sw} represent "near-the-surface" properties. It is unknown how greater material thicknesses would have affected the relations produced in this study.

Analysis of the results of this study also uncovered interesting relations among the key physical variables, ρ_c, f_f, and k_v, and their effect on interlaminar shear strength. It can evidently be concluded that for low void contents, $k_v < 8\%$, the fiber weight fraction, f_f, had relatively greater influence on τ_{il} than k_v. In our correlations of ultrasonic and physical measurements, the data persistently separated into two distinct groups. One group was associated with specimens having <1% void content, the other with >4% void content. In addition we noticed a transition in mechanical modulus (represented by $\rho_c v^2$) as the void content increased from ~1% to ~4%. Data for each transitional specimen were found to be in one of the two groups mentioned above.

Photomicrographs of the short beam shear test specimens showed that there were two distinct fracture modes. In one there was evidence of flexure and fiber tearing, in the other there was only evidence of interlaminar shear. Specimens that were members of the two groups mentioned above belonged to one or the other group in accordance with the fracture mode. Care must be exercised in forming conclusions since there is no way of determining whether shear occurred first followed by tensile failure or visa versa. Interlaminar shear strength measurements do depend on the order of failure. In the present instance only deductive judgements could be made in lieu of actually observing the failure sequence.

Given the results obtained in this and prior studies it seems that stress wave propagation during failure of composites is pivotal,[15-18]. Actual or simulated stress waves probably respond to the same physical factors that either inhibit or promote crack growth. Figure 14 demonstrates how the principle material variables, e.g., ρ_c and f_f, in this study affected the stress wave propagation factor. One can suppose that crack nucleation energy may be dissipated either by crack extension or by propagation of stress waves away from potential nucleation sites. A composite with high values of ε_{sw} would thus exhibit higher strength because stress wave dissipation of energy is enhanced by the same features that increase ε_{sw}. Conversely, low values of ε_{sw} would indicate that fracture energy is likely to concentrate near crack nucleation sites and induce crack growth.

G. CONCLUSION

In this study we examined the interrelation of various factors that influence the mechanical strength properties of a particular unidirectional composite material: graphite fiber in a polyimide matrix. The interlaminar shear strength was selected as a sensitive indicator of strength variations due to material property variations. The pertinent physical variables in this investigation were composite density, fiber weight fraction, and void content. This paper introduced methods and results associated with a new acoustic-ultrasonic technique. The technique involved the injection of simulated stress waves to evaluate composite strength.

Our findings demonstrated the following points:

(1) Ultrasonic measurements can apparently provide a nondestructive means for predicting or estimating interlaminar shear strength of fiber composite laminates (such as those involved in this study).

(2) Acoustic-ultrasonic and physical test methods used in this study are complementary (e.g., the combined methodologies revealed more information than would otherwise have been readily available).

(3) A quantity termed the stress wave factor was found to correlate strongly with interlaminar shear strength as well as with physical properties that determine strength (indicating the importance of stress wave transmission by fibers in determining composite strength).

APPENDIX A

PANEL FABRICATION

The fiber-resin system selected for this study consisted of type AS graphite fiber and 1500 molecular weight PMR polyimide resin. Eleven 12-ply unidirectional panel laminates were made.

Each ply was cut from prepreg sheets which were made by drum-winding Hercules AS graphite fibers and impregnating the wound fibers with a PMR-15 monomer solution. Fiber tows with 10,000 fibers per tow were wound with a pitch of 3 tows per cm (7 tow/in). The fiber was impregnated with an amount of monomer solution that would yield a cured ply thickness of 0.018 cm (0.008 in) and about 60 percent fiber weight fraction, if no resin flow occurred. The prepreg sheet was air dried for one hour on the drum. It was then heated to 49 C (120 F) on the drum for one hour. This drying procedure reduced the level of volatile content in the prepreg to about 10 percent by weight. The result was a drapable, non-tacky prepreg.

After drying, the prepreg sheets were removed from the drum and cut into 7.62 cm (3 in) by 25.4 cm (10 in) plies with the fiber aligned with the 7.6 cm direction. Twelve plies were stacked unidirectionally and imidized in a preforming cup for three hours at 121 C (250 F). The final cure procedure involved heating a matched metal die set to 232 C (450 F) and inserting the imidized preformed stack. The preform was contained in the die and held under press contact pressure for ten minutes. After this initial dwell time, the cure pressure was applied to the die and the mold temperature was increased to 315 C (600 F) at a rate of about 5.5 C (10 F) per minute. When a temperature of 315 C (600 F) was reached, the pressure and temperature were held for one hour.

A series of laminates were molded using the following cure pressures: 0.689, 1.10, 1.38, 2.07, 3.45, and 5.51 MPa (100, 160, 200, 300, 500, and 800 psi, respectively). Prior tests indicated that this range of cure pressure would produce a significant range of void contents and fiber/resin ratios.

APPENDIX B

THROUGH-THICKNESS VELOCITY AND ATTENUATION

Through-the-thickness velocity, v_ℓ, measurements were made by the pulse-echo overlap method.[19] Because of the small specimen thicknesses a modified version of this method was used.[20] This version involved three, rather than the customary two, successive echoes. This allows more precision in measuring velocity in thin specimens such as those used in this study. The first and second echoes were encompassed in one gate while the second and third were encompassed in a second gate, as indicated in fig. 4(b). The continuous wave oscillator frequency was then adjusted to bring all three echoes into coincidence (overlap). The period, p, corresponding to the oscillator frequency is a measure of the time interval needed for sound to traverse twice the specimen thickness, t. Velocity is given by $v_\ell = p/2t$. This velocity is that of longitudinal waves traveling in a direction normal to the specimen surface and also to the fibers.

The attenuation coefficient was determined by measuring the exponential decay constant for multiple echo reverberations in the specimen thickness direction. The method is diagrammed in figs. 4(c) and (d). A calibrated exponential waveform is synchronized with and superimposed on the ultrasonic echo field on an oscilloscope screen. The exponential waveform consists of symmetrical positive and negative halves to fully envelope the positive and negative peaks of the ultrasonic echoes. Once the exponential is matched to the echo peaks, the decay time constant, c (in Nepers per μs), is determined. The quantity c is combined with the previously measured velocity v_ℓ to obtain the attenuation coefficient α_ℓ, where $\alpha_\ell = c/v_\ell$.

Through-the-thickness ultrasonic velocity and attenuation measurements were made with one piezoelectric transducer performing both as a sender and receiver. It had a nominal center frequency of 2.25 MHz. The longitudinal through-the-thickness velocities quoted herein, v_ℓ, may be taken as approximately the 2 MHz-phase velocity component.

APPENDIX C

SURFACE-PARALLEL VELOCITY

The method for measurement of ultrasonic wave velocity parallel to the specimen was similar to that described in[4,5]. In this case, ultrasonic waves are initiated by injecting longitudinal pulses into the specimen with a contact transducer as indicated in fig. 5(a). Because of mode conversion the waves emanating from the contact area are complex and have both transverse and longitudinal components. A receiving transducer is positioned on each side of the sender. The three transducers are

aligned so that the velocity measured is that of waves traveling in a direction normal to the fibers. The spacing of the transducers is unequal. The difference in spacing is s and the consequent difference in wave front arrival time is m. The surface-parallel velocity v_s is given by $v_s = s/m$.

The essence of this method is that of finding m and s. The latter quantity is determined by using the waveguides shown in fig. 5 and by careful measurement of the spacing difference. The waveguides serve as delay lines (that are long compared to the path difference s) to eliminate uncertainties in the path length after the waves are coupled into the pick-up contacts (cones). To determine m the first-arriving wavefront is electronically delayed. The delay time is changed until the two wavefronts are superimposed on an oscilloscope screen. When the superposition is accomplished, the delay interval m is read from a counter-timer display.

The input or sending transducer used for these measurements is identical to the one used for stress wave simulation, described in Appendix C. The velocity v_s is a phase velocity for a wave train with a principal frequency of roughly 1 MHz. Our analysis of these waves indicates that they are essentially transverse. For this reason is assumed that $\rho_c v_s^2$ is proportional to the inter-laminar shear modulus.

APPENDIX D

STRESS WAVE SIMULATION MEASUREMENTS

The method described herewith is applied to one area at a time, and it generates a number associated with that area. This number is termed the "stress wave factor".

A sending transducer injects a repeating series of ultrasonic pulses into the material. Each of these pulses produces simulated stress waves that mimic acoustic emission events in the material.[6,7] A receiving transducer intercepts some of the simulated stress wave energy that radiates from the point of injection.

The stress wave factor value generated for each test area depends on the wave propagation direction relative to the fibers. Other factors that influence the magnitude of the value are fiber/resin ratio, voids, delaminations, etc. The number generated is a purely relative one that will differ for substantially different specimen geometries, i.e., widths, thicknesses, etc.

The transducer configuration for simulation of stress waves and measurement of the stress wave factor is illustrated in fig. 6. Stress wave simulation was accomplished with a 2.25 MHz piezoelectric transducer coupled directly to the specimen surface. The receiving transducer was a piezoelectric acoustic emission transducer having a resonant frequency of approximately 0.6 MHz and an effective bandwidth of roughly 1 MHz.

The sending transducer injects longitudinal waves into the specimen. In the zone of injection mode conversion effects occur. The waves emanating from this zone are therefore complex and have both transverse as well as longitudinal components. The receiver is coupled to the surface through a waveguide. The waveguide effectively transmits only the longitudinal component of the wave that is coupled into it. The waveguide also serves as a delay line that separates the received signal from the input pulse for analytical purposes.

The signals arriving at the receiver resemble "burst" type acoustic emission events. After traveling through the composite, these simulated stress waves bear the imprints of dispersion and other effects that might alter an actual stress wave emanating from the injection zone. The simulated stress waves are repeated at a fixed rate r. The received signal roughly resembles a decaying sinusoid. Each successive "burst" is identical to its predecessors. After amplification, the received signals are sent to a counter that counts the number of oscillations n in each burst exceeding a fixed threshold voltage. The counter is reset automatically after a predetermined time interval g and the previous count is held in a memory and digitally displayed. The displayed count assumes a constant value soon after the specimen is coupled to the probes. The number that is displayed is $\epsilon_{sw} = grn$, the stress wave factor.

Obviously, the number ϵ_{sw} is arbitrary and depends on factors such as signal gain, reset time, threshold voltage, repetition, and so forth. All these factors are, however, kept constant for any series of measurements so that ϵ_{sw} reflects only the material variations of the specimens tested. Our view is that ϵ_{sw} is proportional to transmitted stress wave energy. This is based on the assumption that the number of oscillations in each burst is proportional to its energy content.

H. REFERENCES

1. J. R. Zurbrick, J. Test. Eval., Vol. 1 (1973) p. 13.
2. D. E. W. Stone and B. Clark, Non-Destr. Test., Vol. 8 (1975) p. 137.
3. B. R. Jones and D. E. W. Stone, Non-Destr. Test., Vol. 9 (1976) p. 71.
4. C. H. Hastings, E. F. Olster, and S. A Lopilato, "Development and Application of Nondestructive Methods for Predicting Mechanical Properties of Advanced Reinforced Nonmetallic Composites," AVSD-0183-73-CR, Avco Corp. (AD-771774;AFML-TR-73-157), May 1973.
5. A. W. Schultz, SAMPE Q., Vol. 2 (1971) p. 31.
6. D. M. Egle and A. E. Brown, Test. Eval., Vol. 4 (1976) p. 196.
7. M. Fuwa, A. R. Bunsell, and B. Harris, J. Appl. Phys., Vol. 9 (1976) p. 353.
8. 1973 Annual Book of ASTM Standards, D 2344-72, Part 26, Am. Soc. Test. Mater. 1973, p. 413.
9. R. J. Jones, R. W. Vaughn, and E. A. Burns, "Thermally Stable Laminating Resins," TRW-16402-6012-RO-00, TRW Systems Group, Feb. 1972, p. 79; also NASA CR-72984.
10. 1973 Annual Book of ASTM Standards, D 2734-70, Part 26, Am. Soc. Test. Mater., 1973, p. 768.
11. E. Cilley, D. Roylance, and N. Schneider, Composite Materials: Testing and Design, STP-546, Am. Soc. Test. Mater., 1973, p. p. 237.
12. I. Petker, SAMPE Q., Vol. 3 (1972) p. 7.
13. L. B. Greszczuk, Composite Reliability, STP 580, Am. Soc. Test. Mater., 1975, p. 311.
14. L. B. Greszczuk, 22rd Annual Technical Conference on Reinforced Plastics International, Soc. Plast. Ind., Inc., 1967, p. 20-A.1.
15. H. J. Sutherland and D. E. Munson, J. Compos. Mater., Vol. 10 (1976) p. 118.
16. A. B. Schultz and D. N. Warwick, J. Compos. Mater., Vol. 5 (1971) p. 394.
17. E. C. Goeke and F. A. McClintock, J. Appl. Phys., Vol. 46 (1975) p. 4671.
18. P. J. Cavano, "Resin/Graphite Fiber Composits," TRW-ER-7677F, TRW Equipment Labs., Dec. 1974; also ASA CR-134727.
19. E. P. Papadakis, Crit. Rev. Solid State Sci., Vol. 4 (1973) p. 373.
20. A. Vary, "Correlations Among Ultrasonic Propagation Factors and Fracture Toughness Properties of Metallic Materials," NASA TM X-71889, Mar. 1976.

TABLE I. - MATERIAL PROPERTIES FOR GRAPHITE-POLYIMIDE COMPOSITE SPECIMENS

(AS GRAPHITE AND PMR-15 POLYIMIDE)

Specimen (E-strip)	Cure pressure p, MPa	Composite density ρ_c, g/cm^3	Weight fraction		Void fraction, k_v (%)	Interlaminar shear strength τ_{il}, MPa (ksi)
			Fiber f_f	Resin f_r		
P20E	3.45	1.586	0.632	0.368	0	113.7 (16.5)
P21E	3.45	1.580	.655	.345	1.0	111.6 (16.2)
P22E	1.38	1.552	.615	.385	1.4	98.5 (14.3)
P23E	1.38	1.558	.613	.387	1.0	102.7 (14.9)
P24E	1.10	1.520	.653	.347	4.7	90.3 (13.1)
P25E	5.51	1.586	.651	.349	0	114.4 (16.6)
P26E	.69	1.501	.625	.375	5.0	83.4 (12.1)
P27E	.69	1.495	.619	.381	5.2	81.3 (11.8)
P28E	1.10	1.539	.607	.393	2.0	97.1 (14.1)
P29E	1.10	1.515	.625	.375	4.1	88.9 (12.9)
P30E	2.07	1.575	.626	.374	0	107.5 (15.6)

TABLE II. - NONDESTRUCTIVELY MEASURED PROPERTIES FOR GRAPHITE-POLYIMIDE COMPOSITE SPECIMENS

(AS GRAPHITE AND PMR-15 POLYIMIDE)

Specimen (E-strip)	Velocity through thickness v_ℓ, cm/μs	Velocity surface parallel v_s, cm/μs	Ultrasonic modulus		Attenuation coefficient (thickness) α_ℓ, Np/cm	Stress wave factor, ϵ_{sw}
			Through thickness $\rho_c v_\ell^2 \times 10^2$, g/cm $(\mu s)^2$	Surface parallel $\rho_c v_s^2 \times 10^2$, g/cm $(\mu s)^2$		
P20E	0.257	0.120	10.5	2.28	1.23	2.38
P21E	.255	.122	10.3	2.37	1.35	2.38
P22E	.252	.136	9.9	2.87	1.50	1.36
P23E	.237	.133	8.8	2.76	1.89	1.77
P24E	.223	.154	7.6	3.59	1.86	1.20
P25E	.255	.120	10.3	2.28	1.38	2.79
P26E	.223	.166	7.5	4.11	1.86	.873
P27E	.217	.169	7.0	4.29	2.31	.699
P28E	.234	.143	8.4	3.14	1.98	.736
P29E	.226	.157	7.7	3.72	2.02	.996
P30E	.253	.125	10.1	2.45	1.25	1.82

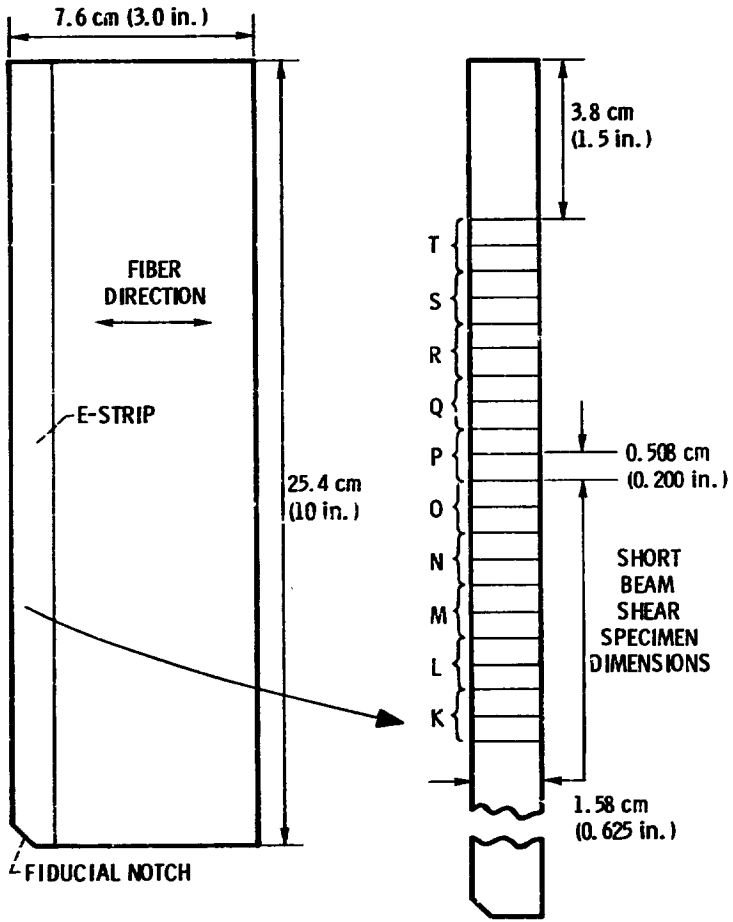

(a) OVERALL PANEL DIMENSIONS. (b) E-STRIP, SPECIMEN SOURCE.

Figure 1. - Laminate panel and E-strip from which short-beam shear specimens were taken. (Panel thickness ranged from 0.231 cm to 0.250 cm.)

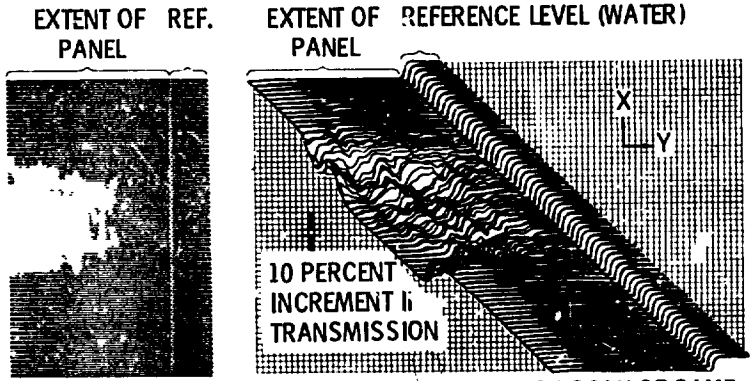

(a) EXAMPLE OF A CONVENTIONAL ULTRASONIC BLACK-WHITE "C-SCAN".

(b) EXAMPLE OF AMPLITUDE SCAN OF SAME OBJECT AS THAT IN FIGURE 2(a). OBJECT IS A FLAT COMPOSITE PANEL SELECTED TO SHOW A RANGE IN ULTRASONIC TRANSMISSION.

Figure 2. - Illustration of various through-transmission ultrasonic scan images indicating variation of transmitted ultrasound due to attenuation by voids and fiber fraction variations in typical graphite-polyimide composite panels.

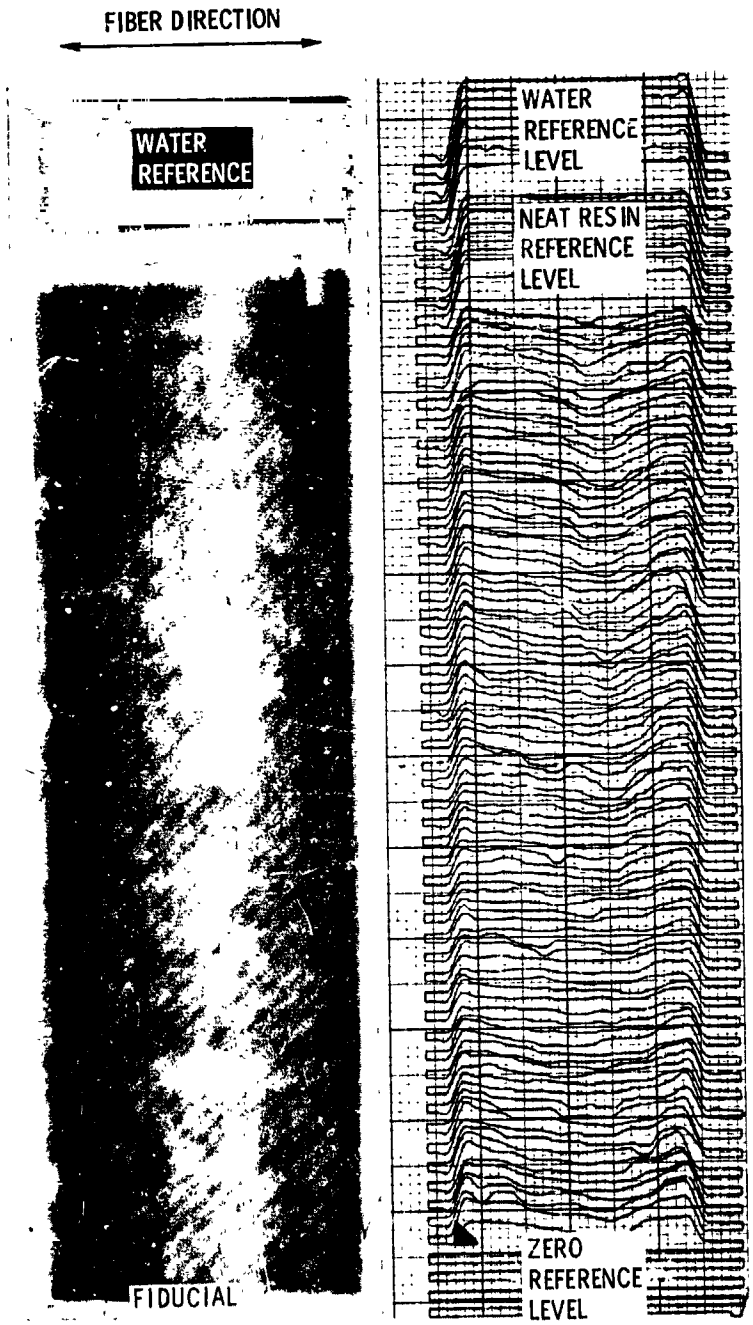

(c) GREYTONE SCAN OF COMPOSITE PANEL USED IN THIS STUDY.

(d) AMPLITUDE SCAN OF COMPOSITE PANEL USED IN THIS STUDY.

Figure 2. - Concluded.

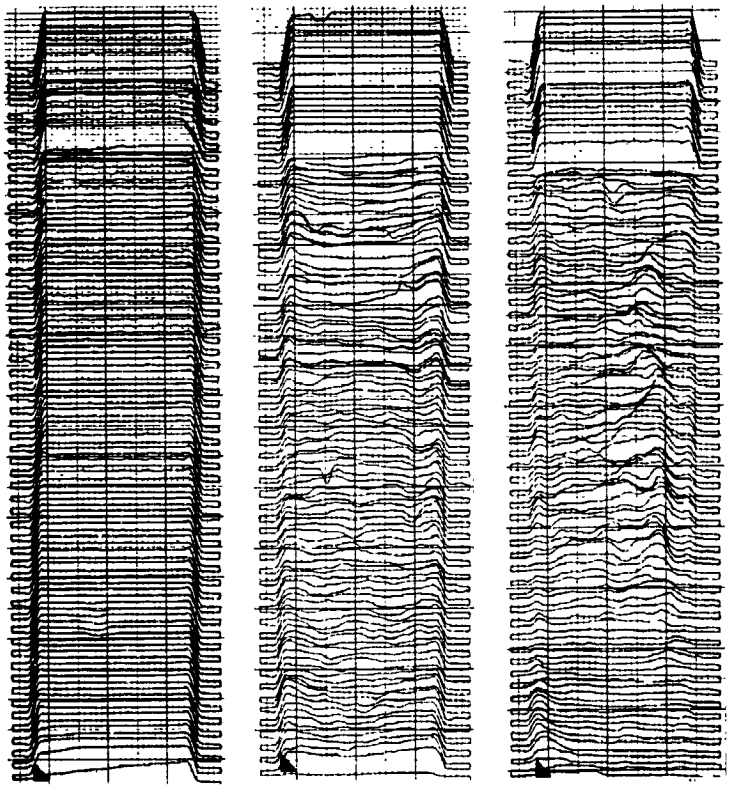

(a) CURE PRESSURE = 3.45 MPa (500 psi). (b) CURE PRESSURE = 1.38 MPa (200 psi). (c) CURE PRESSURE = 1.10 MPa (160 psi).

Figure 3. - Comparison of amplitude ultrasonic scans of graphite-polyimide composite panels formed with three different cure pressures.

LEGEND

S IS THE SYNCHRONIZATION SIGNAL TO THE OSCILLOSCOPE TIME BASE. THIS SIGNAL IS DERIVED FROM THE OSCILLATOR OUTPUT.

X IS THE SIGNAL TO THE OSCILLOSCOPE HORIZONTAL AMPLIFIER. THE AMPLITUDE OF X DEPENDS ON THE OSCILLATOR FREQUENCY. THIS SIGNAL IS USED TO CONVOLVE THE Y SIGNAL, SEE FIG. 4(b).

Y IS THE SIGNAL TO THE OSCILLOSCOPE VERTICAL AMPLIFIER. THE Y SIGNAL CORRESPONDS TO THE ULTRASONIC ECHOES RECEIVED BY THE TRANSDUCER DURING EACH PULSE INTERVAL.

Z IS THE SIGNAL TO THE OSCILLOSCOPE TRACE INTENSIFIER. THE TRACE INTENSITY IS MADE STRONGER FOR PORTIONS OF THE Y SIGNAL THAT ARE BRACKETED WITHIN GATES Z1 AND Z2.

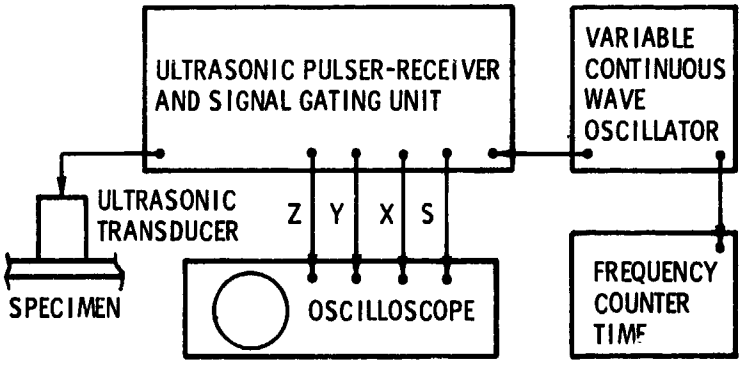

(a) APPARATUS FOR ULTRASONIC VELOCITY MEASUREMENT.

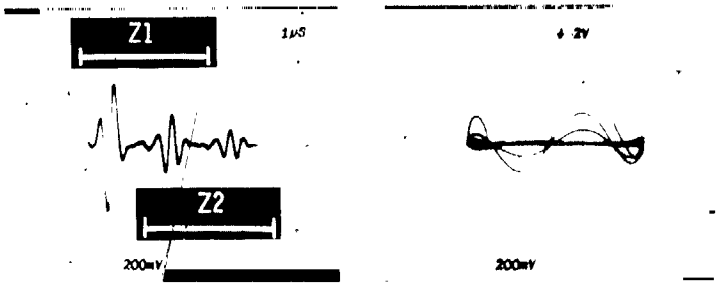

OSCILLOSCOPE TRACE OF Y SIGNAL INDICATING GATES Z1 AND Z2.

Y SIGNAL WITH THREE ECHOES OVERLAPPED.

(b) SIGNALS USED IN VELOCITY MEASUREMENT.

Figure 4. Diagram of apparatus and signal treatment used in ultrasonic velocity and attenuation measurements through the specimen thickness.

LEGEND

S IS THE SYNCHRONIZATION SIGNAL TO THE OSCILLOSCOPE TIME BASE AND TO THE EXPONENTIAL GENERATOR.

Y IS THE SIGNAL TO THE OSCILLOSCOPE VERTICAL AMPLIFIER. THE Y SIGNAL CORRESPONDS TO THE TRAIN OF ECHOES SHOWN IN FIG. 4(d).

E IS THE ± EXPONENTIAL SIGNAL TO THE AUXILIARY VERTICAL AMPLIFIER.

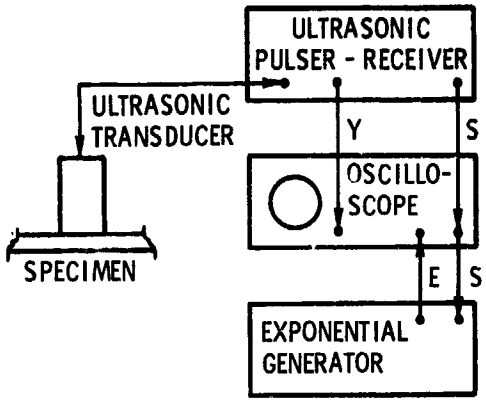

(c) APPARATUS FOR ATTENUATION MEASUREMENT.

OSCILLOSCOPE TRACE SHOWING SIGNAL E SUPERIMPOSED AND MATCHED WITH THE EXPONENTIAL DECAY OF SIGNAL Y.

(d) SIGNALS USED IN ATTENUATION MEASUREMENT.

Figure 4. - Concluded.

LEGEND

S IS THE SYNCHRONIZATION SIGNAL TO THE TIME-BASE (TB) MODULES.

Y IS THE RECEIVED SIGNAL TO THE VERTICAL AMPLIFIER (VA) MODULE CHANNELS.

D IS THE SIGNAL FROM THE TIME BASE DELAY GATES TO THE COUNTER-TIMER (C/T) MODULE.

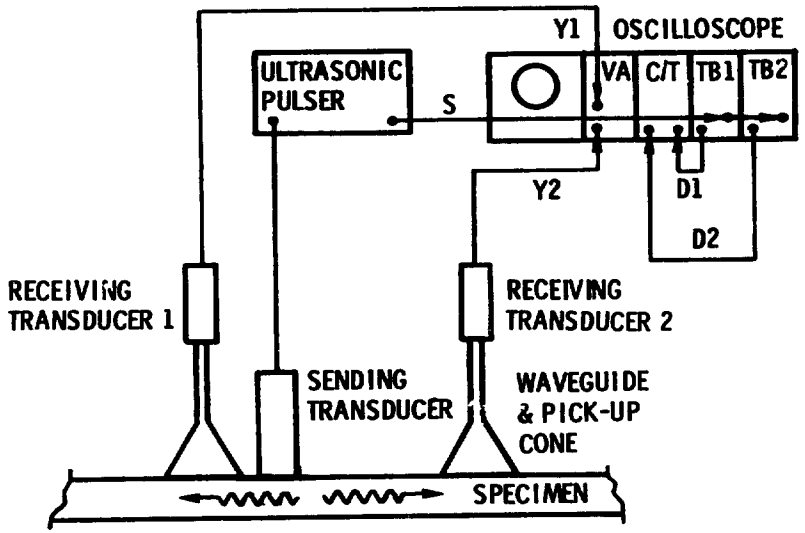

(a) APPARATUS FOR SURFACE-PARALLEL VELOCITY MEASUREMENTS.

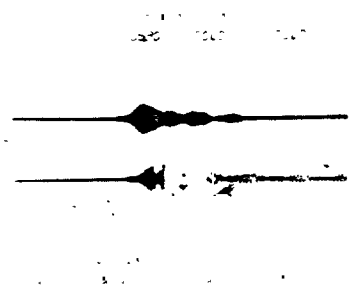

OSCILLOSCOPE TRACE OF SIGNALS Y1 AND Y2, DELAY GATE INTENSIFIED.

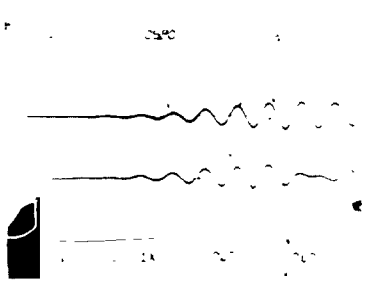

INTENSIFIED PARTS OF Y1 AND Y2 FROM DELAY GATES D1 AND D2.

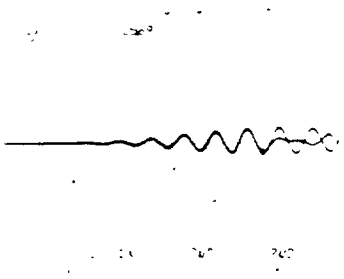

SUPERIMPOSED GATED SIGNALS AND C/T DELAY READOUT DISPLAY (5.6 μs).

(b) SIGNAL TREATMENT FOR SURFACE PARALLEL VELOCITY MEASUREMENTS.

Figure 5. - Apparatus and signal treatment used in measurement of ultrasonic velocity parallel to the specimen surface.

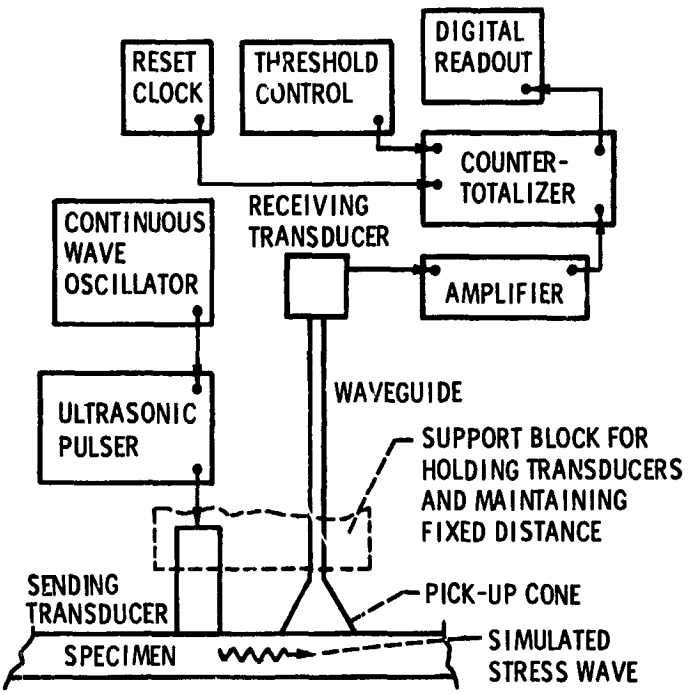

(a) APPARATUS FOR STRESS WAVE SIMULATION & MEASUREMENT.

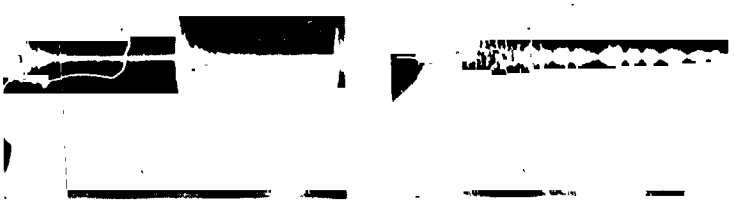

OSCILLOSCOPE TRACE SHOWING CONTINUOUSLY REPEATING BURSTS OF SIMULATED STRESS WAVES.

SINGLE BURST WAVEFORM. THRESHHOLD OF OSCILLATION COUNTS IS ± 0.5 SCALE DIVISION.

(b) SIGNALS USED FOR STRESS WAVE OSCILLATION COUNT.

Figure 6. - Apparatus and signal treatment used for measuring the stress wave propagation factor.

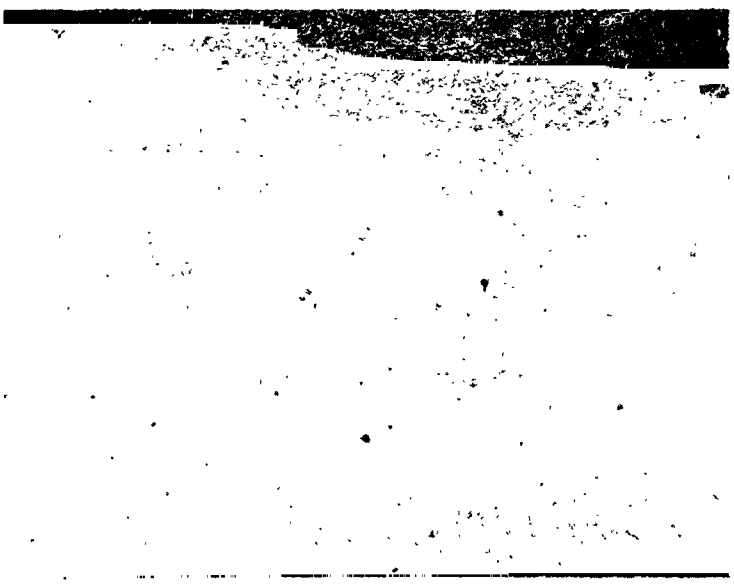

(a) END VIEW OF FIBERS AND VOIDS IN TYPICAL COMPOSITE SPECIMEN, X50. INTERMEDIATE GREY IS RESIN.

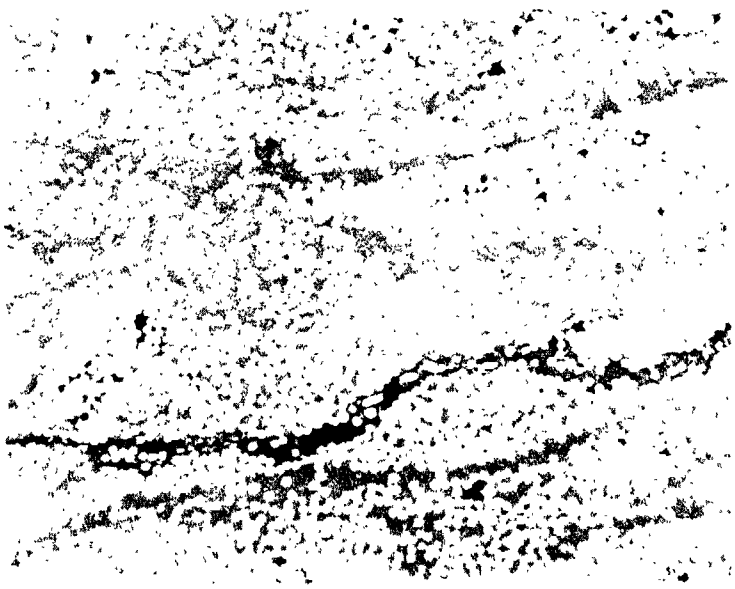

(b) ENLARGEMENT OF PORTION OF FIG. 7(a) SHOWING DETAIL OF VOIDS (DARKEST GREY) AND FIBERS (LIGHTEST GREY), X160.

Figure 7. - Photomicrographs of graphite-polymide composite showing the nature of typical voids and fractures.

(c) EDGE VIEW OF SPECIMEN AFTER SHORT-BEAM SHEAR TEST SHOWING FIBER TEARING ON TENSILE SIDE AND MIDPLANE, X30.

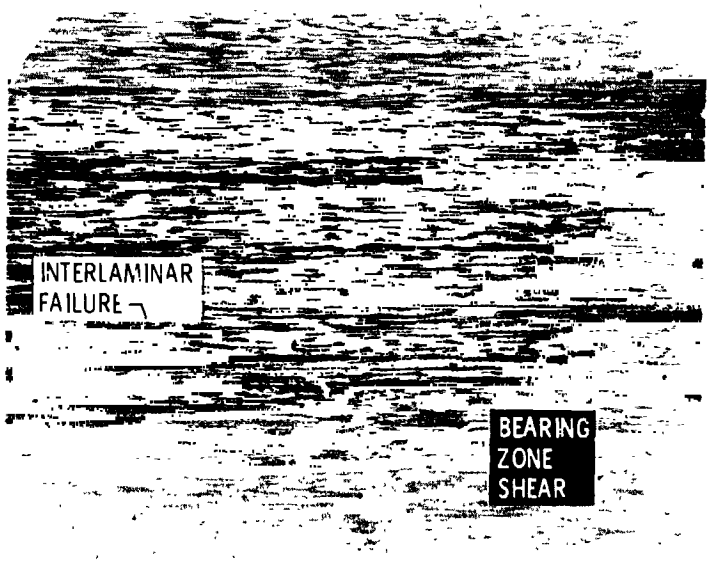

(d) EDGE VIEW OF SPECIMEN AFTER SHORT-BEAM SHEAR TEST IN WHICH FIBER TEARING IS ABSENT AND FAILURE WAS SOLELY BY INTERLAMINAR SHEAR, X30.

Figure 7. - Concluded.

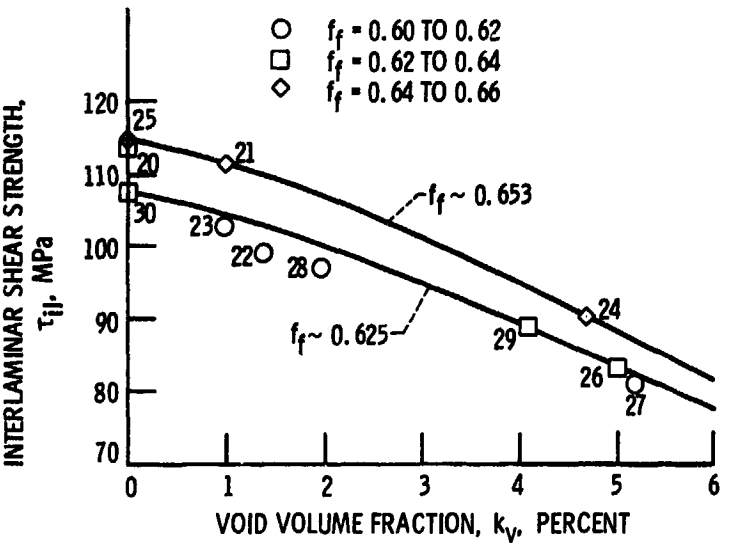

Figure 8. - Effect of variations of void volume fraction and fiber weight fraction, f_f, on interlaminar shear strength for graphite-polyimide composite. (Note that curves are drawn through points having fiber weight fractions that differ by 0.002 or less. The curves intersect for a void volume fraction of roughly 8 percent.)

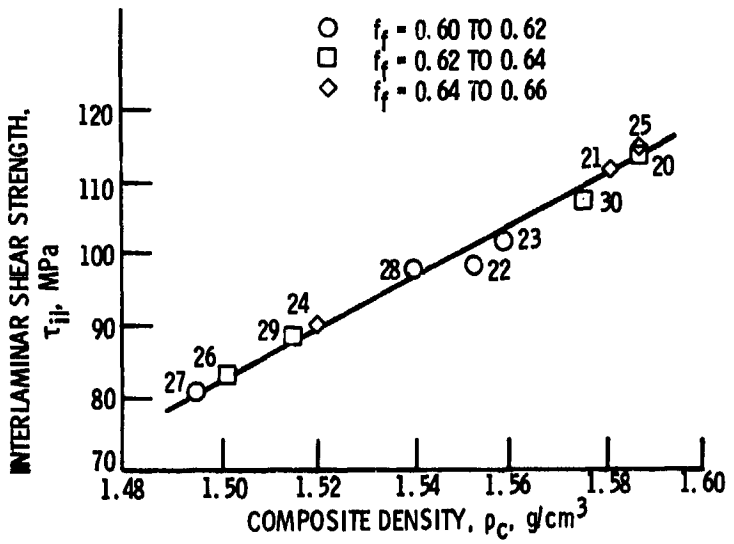

Figure 9. - Effect of composite density on interlaminar shear strength of short-beam shear specimens of graphite-polyimide composite.

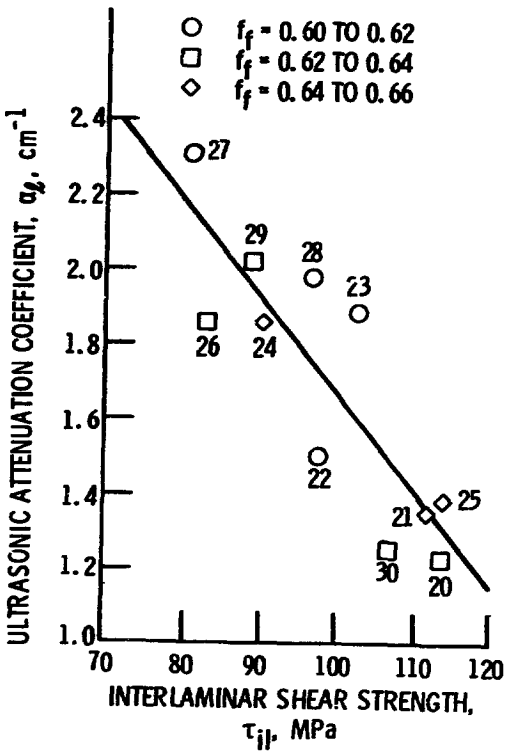

Figure 10. - Correlation between ultrasonic attenuation coefficient and interlaminar shear strength for graphite-polyimide composite. Attenuation was measured at a center frequency of approximately 2 MHz.

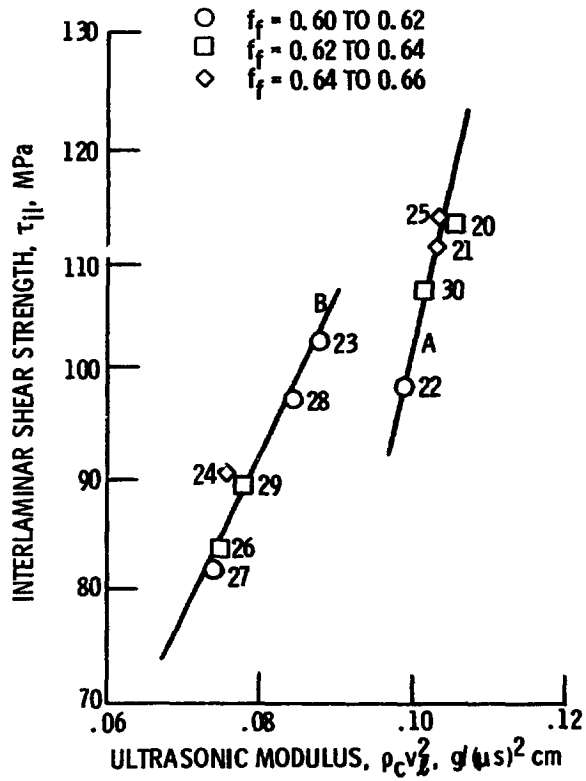

Figure 11. - Correlation between interlaminar shear strength and ultrasonic modulus for graphite-polyimide composite. Based on through-thickness velocity measurement at a center frequency of approximately 2 MHz.

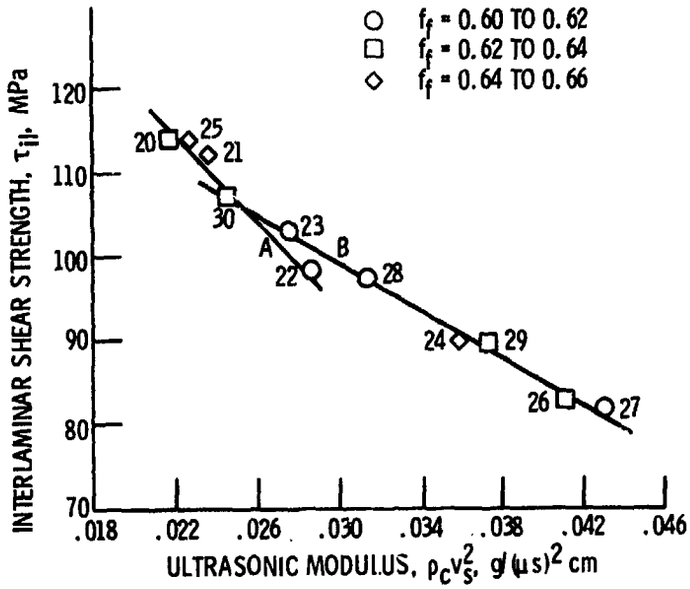

Figure 12. - Correlation between interlaminar shear strength and ultrasonic modulus for graphite-polyimide composite. Based on surface-parallel velocity measurement at a center frequency of approximately 1 MHz.

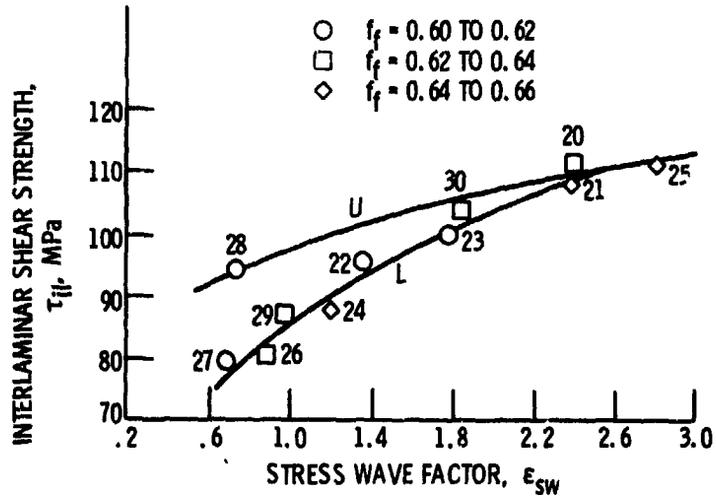

Figure 13. - Correlation of interlaminar shear strength with stress wave factor for graphite-polyimide composite. Stress wave factor was measured for waves in the range from 0.1 to 1.0 MHz propagating parallel to the laminate surface and perpendicular to the unidirectional fibers.

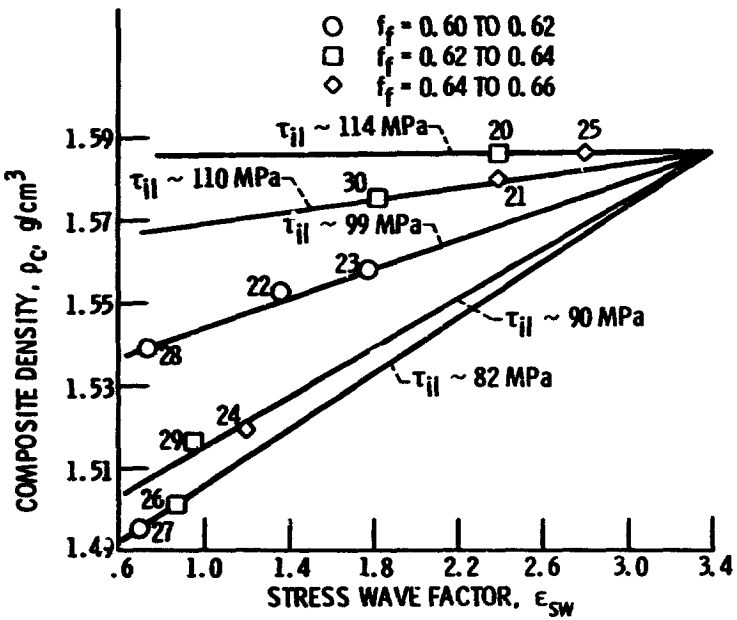

Figure 14. - Covariation of composite density and interlaminar shear strength with stress wave factor for graphite-polyimide composite.

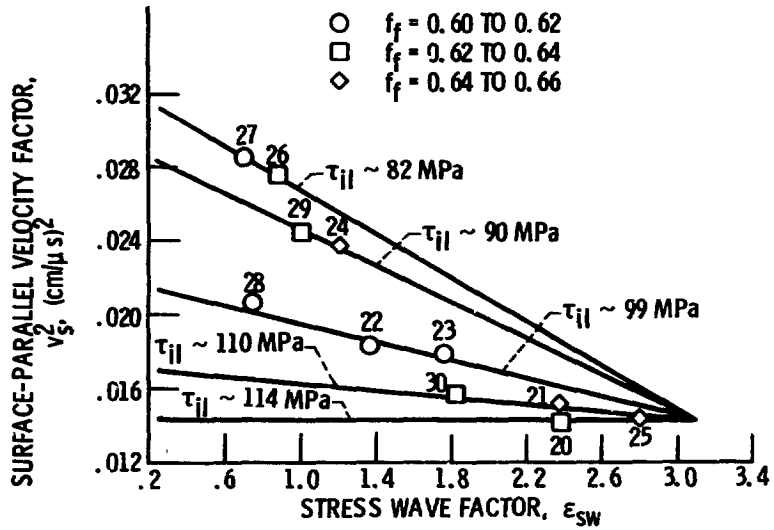

(a) COVARIATION OF INTERLAMINAR SHEAR STRENGTH WITH VELOCITY AND STRESS WAVE FACTOR.

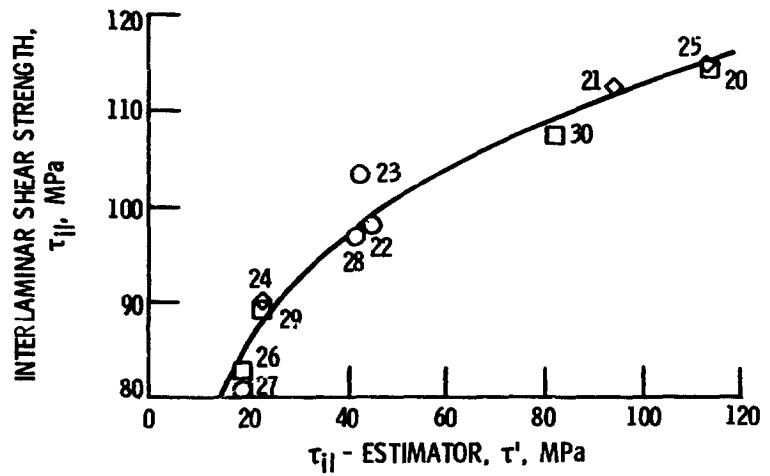

(b) CORRELATION BETWEEN INTERLAMINAR SHEAR STRENGTH AND ITS ESTIMATOR, τ', BASED ON FIGURE 15(a).

Figure 15. - Empirical relations for estimating interlaminar shear strength based on velocity, v_s, and stress wave factor, ϵ_{sw}, for graphite-polyimide composite.

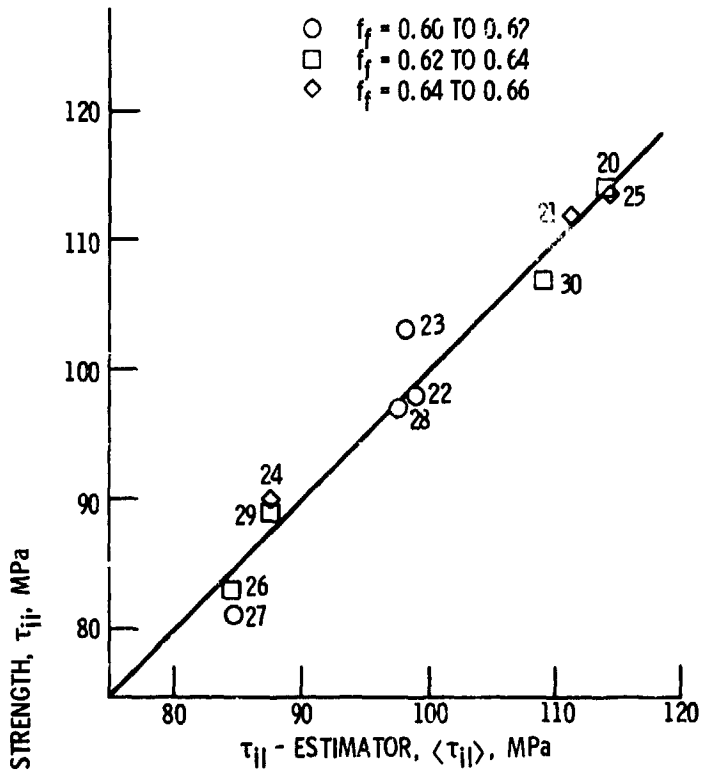

(c) CORRELATION BETWEEN INTERLAMINAR SHEAR STRENGTH AND ITS ESTIMATOR, $\langle\tau_{ll}\rangle$, BASED ON FIGURE 15(b).

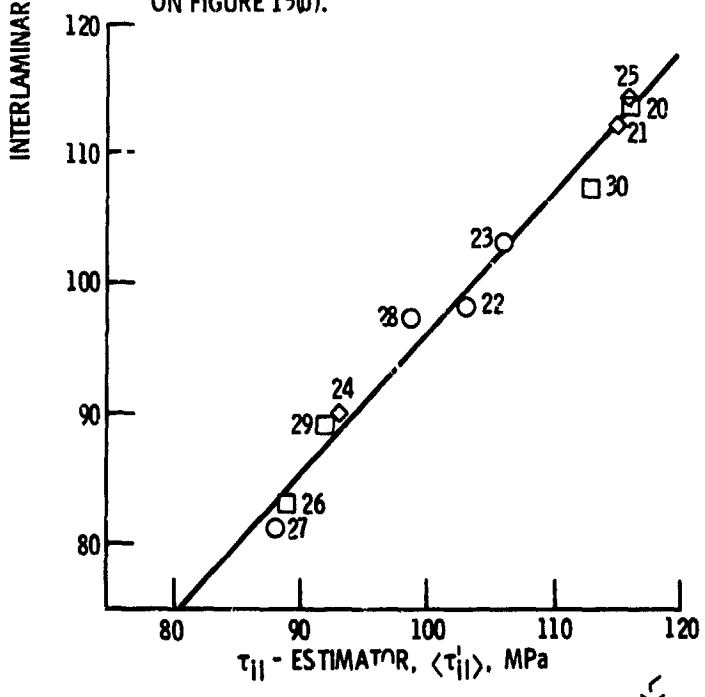

(d) CORRELATION BETWEEN INTERLAMINAR SHEAR STRENGTH AND ITS ESTIMATOR, τ'_{ll}, BASED ON EQUATION (6).

Figure 15. - Concluded